Molecular Vision 2016; 22:82-99 <http://www.molvis.org/molvis/v22/82>
Received 17 September 2015 | Accepted 27 January 2016 | Published 29 January 2016

Scleral fibroblast response to experimental glaucoma in mice

Ericka N. Oglesby,[1] Gülgün Tezel,[2] Elizabeth Cone-Kimball,[1] Matthew R. Steinhart,[1] Joan Jefferys,[1] Mary E. Pease,[1] Harry A. Quigley[1]

[1]Glaucoma Center of Excellence, Wilmer Ophthalmological Institute Department of Ophthalmology, Johns Hopkins University, Baltimore, MD; [2]Department of Ophthalmology, Columbia University, New York, NY

Purpose: To study the detailed cellular and molecular changes in the mouse sclera subjected to experimental glaucoma.
Methods: Three strains of mice underwent experimental bead-injection glaucoma and were euthanized at 3 days and 1, 3, and 6 weeks. Scleral protein expression was analyzed with liquid chromatography coupled with tandem mass spectrometry (LC-MS/MS) using $^{16}O/^{18}O$ labeling for quantification in 1- and 6-week tissues. Sclera protein samples were also analyzed with immunoblotting with specific antibodies to selected proteins. The proportion of proliferating scleral fibroblasts was quantified with Ki67 and 4',6-diamidino-2-phenylindole (DAPI) labeling, and selected proteins were studied with immunohistochemistry.
Results: Proteomic analysis showed increases in molecules involved in integrin-linked kinase signaling and actin cytoskeleton signaling pathways at 1 and 6 weeks after experimental glaucoma. The peripapillary scleral region had more fibroblasts than equatorial sclera (p=0.001, n=217, multivariable regression models). There was a sixfold increase in proliferating fibroblasts in the experimental glaucoma sclera at 1 week and a threefold rise at 3 and 6 weeks (p=0.0005, univariate regression). Immunoblots confirmed increases for myosin, spectrin, and actinin at 1 week after glaucoma. Thrombospondin-1 (TSP-1), HINT1, vimentin, actinin, and α-smooth muscle actin were increased according to immunohistochemistry.
Conclusions: Scleral fibroblasts in experimental mouse glaucoma show increases in actin cytoskeleton and integrin-related signaling, increases in cell division, and features compatible with myofibroblast transition.

The sclera and the optic nerve head (ONH) are directly affected by the stress induced by intraocular pressure (IOP), producing known detrimental effects on retinal ganglion cells (RGCs) and their axons in glaucoma as the axons pass through the optic nerve head [1-3]. The stress of IOP is transmitted to RGC axons through the sclera to the ONH connective tissues, which are a site of glaucoma damage [4]. The sclera expands or contracts with IOP fluctuation in a well-recognized pressure–volume relationship in healthy eyes [5]. The sclera is regionally configured to resist strain where it is highest, at the peripapillary sclera [6]. The scleral connective tissues consist of alternating and interwoven lamellae of collagen, elastin, and proteoglycans [7,8], with 20% of the human scleral thickness consisting of cellular lamellae containing scleral fibroblasts [9]. This biomechanical behavior has been extensively studied in experimental glaucoma eyes in the mouse [10] and monkey [11-13] and in glaucomatous and healthy human eyes [14]. Human glaucoma donor eyes with RGC loss are measurably stiffer than control eyes, and experimental mouse and monkey glaucoma eyes become stiffer with chronic increased IOP. Age-related, ethnic, and genetic differences in scleral composition may also contribute to glaucoma susceptibility. The ONH and peripapillary scleral elastin differs between individuals of African descent and European descent, perhaps representing a risk factor for higher open angle glaucoma (OAG) prevalence in individuals of African descent [15]. The decrease in axial length with age is also indicative of a scleral remodeling process [16]. Molecularly, mutations in the lysyl oxidase-like protein 1 *(LOXL1*, Gene ID:4016, OMIM 153456) gene are associated with exfoliation glaucoma [17], a common subgroup of OAG, in which abnormalities in posterior ocular connective tissues are present [18].

Intrinsic scleral features and the scleral response to chronic IOP elevation are related to susceptibility to RGC loss in mouse models [19]. CD1 mice are more susceptible to RGC loss than the B6 strain [20] and a mouse strain with a mutation in collagen 82 (Aca23) was less susceptible than the B6 strain [21]. In a study of these mouse strains, resistance to damage was associated with reduced axial elongation after IOP elevation [22]. Further evidence of the relevance of the scleral extracellular matrix response in glaucoma is that less susceptible B6 mice had thicker peripapillary sclera at baseline and did not undergo uniform scleral thinning with experimental glaucoma as did the more susceptible CD1 mice [23]. The usual circumferential pattern of collagen fibrils in the peripapillary sclera widened significantly in damaged

Correspondence to: Ericka Oglesby, Johns Hopkins Wilmer Eye Institute, Smith Building, 400 North Broadway, Baltimore, MD 21287, Phone: +1 (410) 955 3332; FAX: +1 (443) 287 2711; email: eoglesb1@jhmi.edu

glaucoma eyes, and there was a greater number of small diameter collagen fibrils in the glaucoma mouse sclera [23]. Experimental glaucoma also caused a decrease in the capacity of the sclera for diffusion of large molecules, with greater decreases in the peripapillary area than in the equatorial sclera and lower diffusion rates in Aca23 and B6 mice than in CD1 mice, which paralleled their relative susceptibility to experimental glaucoma injury [24]. Consistent with this finding, the non-fibrillar component of sclera also significantly decreased in volume in experimental glaucoma eyes. Treatment of mice with losartan, an inhibitor of angiotensin 1 receptors, dramatically decreased experimental glaucoma damage, with several indicators pointing to modification of the scleral response as central to the beneficial effect [25].

Fibroblasts make up 25% of scleral thickness in mice and are likely to be instrumental in producing the sclera's response to glaucoma. The fibroblast-containing lamellae expanded significantly in the experimental glaucoma mouse sclera [23]. We have developed techniques for studying scleral responses in whole tissue samples, using confocal microscopy and proteomic analysis. Experimental bead-injection glaucoma was produced in three mouse strains, as part of a series of studies evaluating strain-specific features relevant to glaucoma. This report focuses on overall changes common to all three groups of mice in the number of fibroblasts, their rate of multiplication, histological changes in important cellular and extracellular components, and alterations in protein expression. By analyzing which alterations in protein content are associated with experimental glaucoma damage and with susceptibility to its injury, we may identify features that are likely to be useful as diagnostic risk factors in human glaucoma eyes, as well as pointing to candidate molecules for glaucoma susceptibility that affect connective tissue structural elements. Furthermore, modulation of scleral biomechanical properties could be a novel neuroprotective approach for glaucoma.

METHODS

Animals: C57BL/6J (B6) mice were acquired from Jackson Laboratories (Bar Harbor, ME), and CD1 mice were acquired from Charles River, Inc. (Wilmington, MA). The founder mice of the Aca23 type, which were of a B6 base strain, were provided by Drs. Puk and Graw [21]. All mice were 2–5 months of age. All animals and experiments were conducted in accordance with the ARVO Statement for the Use of Animals in Ophthalmic and Vision Research. All protocols were approved and monitored by the Johns Hopkins University School of Medicine Animal Care and Use Committee. A total of 148 mice were studied, consisting of 33 B6 mice, 78 CD1 mice, and 11 homozygous Aca23 mutants and 12 of their wild-type (WT) littermates.

Experimental glaucoma model, axial length, and axon counts: To induce experimental glaucoma, beads were injected into the anterior chamber unilaterally under intraperitoneal anesthesia (50 mg/kg ketamine, 10 mg/kg xylazine, and 2 mg/kg acepromazine), along with topical anesthesia (0.5% proparacaine hydrochloride eye drops; Akorn Inc., Buffalo Grove, IL). The fellow eye was left untreated as a control. The protocol used was the 4+1 bead injection method [19], consisting of 2 µl of 6 µm diameter beads (Polybead Microspheres®; Polysciences, Inc., Warrington, PA) and then 2 µl of 1 µm diameter beads, followed by 1 µl of viscoelastic compound (10 mg/ml sodium hyaluronate, Healon; Advanced Medical Optics Inc., Santa Ana, CA). IOP was measured immediately after injection, and at 3 days, 1 week, 2 weeks, and 6 weeks, using the Tonolab tonometer (TioLat, Inc., Helsinki, Finland). At the times indicated, the mice were euthanized with exsanguination under the indicated intraperitoneal anesthesia.

For axial length measurements, the globes were removed after euthanasia was performed, and IOP was set at 15 mmHg with a needle placed in the anterior chamber and connected to a fluid-filled reservoir to standardize the conditions for axial length and width measurements. Length was measured from the center of the cornea to a point just temporal to the optic nerve. Nasal to temporal width was measured at the largest dimension of the equator. Both measures were taken using a digital caliper (Instant Read Out Digital Caliper, Electron Microscopy Sciences, Hatfield, PA).

Axon loss in optic nerve sections was estimated in immersion-fixed optic nerve cross sections with a quantitative sampling technique [25,26]. After primary aldehyde fixation and post-fixation in 1% osmium, the nerves were embedded in epoxy resin and sectioned at 1 µm. Low power images of the nerves were taken to determine the nerve area. In 100X images, the axon density per mm^2 number was quantified by masked observers, editing non-axonal elements (Metamorph Image Analysis software, Cool Snap camera, Molecular Devices, Downington, PA). For each nerve, five fields were randomly sampled (9% of the overall nerve area). The average axon density was multiplied by the individual nerve area to estimate the axon number [26]. Experimental eyes were compared to the mean axon number in the pooled, fellow eye nerves of the appropriate strain, age, and tissue fixation to yield the percent axon loss.

Tissue preparation for proteomic analysis: Proteomics study of the sclera was conducted on a combined total of 45 B6 and Aca23 WT mice, 30 CD1, and 11 Aca23 mutants. The

anterior structures, retina, and choroid were removed, and whole scleras from five to seven experimental eyes or five to seven control eyes per time point were pooled for analysis. The scleras were frozen at −80 °C. The mice were tested in two groups: An initial cohort of CD1 and B6 mice were euthanized 6 weeks after experimental glaucoma induction (comprising two sets of data, one from each strain). A second group of proteomic studies included CD1 and B6 mice as well as Aca23 mice euthanized at 1 week and 6 weeks after experimental glaucoma. Thus, the second group had six sets of data, two from each of the three strains of mice at two time points. The second group thus served as a validating replicate for the first 6-week data sets in the CD1 and B6 mice.

Quantitative LC-MS/MS analysis: Scleral proteins were extracted with a lysis buffer containing 50 mM HEPES-KOH pH 8.0, 100 mM KCl, 2 mM EDTA, 0.10% NP-40, 2 mM dithiothreitol, 10% glycerol, and protease and phosphatase inhibitors as previously described [27-29]. Protein concentrations were measured with a Bradford assay (Bio-Rad, Hercules, CA). Protein samples were analyzed with liquid chromatography-tandem mass spectrometry (LC-MS/MS) using isotope labeling ($^{16}O/^{18}O$ labeling [30-33]) for relative quantification as we previously described [25]. Briefly, protein lysates were desalted and dried after digestion with 0.4 µg/µl trypsin (Promega, Madison, WI). For trypsin-catalyzed ^{16}O-to-^{18}O exchange/labeling, the samples were dissolved in a solution containing 50 µl of 50 mM Tris buffer (pH 7.8), 5 mM $CaCl_2$, and 1 µg trypsin prepared either in normal or ^{18}O labeled water (Sigma-Aldrich, St. Louis, MO). Following incubation at 37 °C for 24 h, the samples were heated to 100 °C for 10 min, acidified with 25 µl 5% formic acid (FA), and desalted with the C_{18} spin column (Nest Group, Southborough, MA). ^{18}O- or ^{16}O-labeled samples were then mixed and fractionated with strong cation exchange (SCX) and C_{18} resin using a reversed-phase (RP) gradient as previously described [26-28]. The samples dissolved in 25 µl of loading buffer were loaded on an SCX cartridge, and step-wise eluted with 20 µl of 15 SCX buffers (containing ammonium acetate/acetic acid) of different ionic strength and pH. Eluted fractions were dissolved in 10 µl 5% acetonitrile (ACN)/0.1% FA and analyzed with a nanoAcquity (Waters, Milford, MA)-LTQ Orbitrap XL (Thermo Scientific, San Jose, CA) system in data-dependent scan (DDS) mode. An in-house capillary column (0.1 × 130 mm column packed with 3.6 µm, 200 Å Aeris XB-C_{18}) and a gradient with 0.1% FA and ACN/0.1% FA were used for separation.

Data files from experimental glaucoma pooled samples were compared to fellow eye control pooled samples at a given time point in terms of the relative amounts of each protein by searching against the most current version of the Proteome Discoverer v1.4 database (Thermo Scientific). At least three high-confidence peptide matches were required for protein identification (false discovery rate <1%). Proteins matched with the same peptides were reported as one protein group. Relative abundances for differentially labeled peptides were calculated from peak areas of their monoisotopic peaks and reported as heavy-to-light ($^{18}O/^{16}O$) ratios. Changes of at least twofold (increase or decrease) were required to be considered significant changes, as, based on the accuracy of mass spectrometry-based quantification, a minimum of 1.3-fold to twofold protein expression change is a meaningful cutoff for biologic significance [34,35].

Similar to our previous studies [26,27], the Ingenuity Pathways Analysis system (Ingenuity Systems, Mountain View, CA) was used for bioinformatics analysis of the proteomics data sets to search functional patterns from the Ingenuity Pathways Analysis library. Canonical pathway analysis identified the pathways significantly associated with our data sets with the right-tailed Fisher's exact test. Proteomic analysis compared the protein expression levels in the experimental glaucoma to the control sclera for each strain at 1 week or 6 weeks. For this report, any reference to changes in expression refer specifically to protein expression levels.

Immunoblot: For confirmation of proteomic data, additional mouse scleral samples were studied with quantitative western blot analysis as previously described [26-28]. We tested for four of the proteins that were more highly and consistently changed by glaucoma at 1 week after glaucoma induction: spectrin, myosin, integrin, and actinin. Other frequently increased proteins for which immunoblot analysis was technically not possible were studied with immunohistochemistry.

Briefly, the eyes were excised, and the tissues were separated and frozen in a slurry of dry ice/ethanol in microcentrifuge tubes. Proteins were extracted using the Total Protein Extraction Kit (EMD Millipore, Inc., Billerica, MA). Tissues were placed in extraction solution and macerated with a motorized pestle (Kimble-Kontes, Hainesport, NJ), taken through freeze-thaw cycles, and centrifuged to remove undissolved material. Sample protein concentrations were determined using the EZQ Protein Quantification Kit (Life Technologies, Grand Island, NY). Equal protein amounts for each sample were run on 4–10% Bis-Tris gels (Novex, Thermo Fisher) and then wet transferred to polyvinylidene difluoride membranes (Bio-Rad, Hercules, CA). Membranes were washed in PBS (1X; 154 mM NaCl, 1.5 mM KH_2PO_4, 5.1 mM Na_2HPO_4, pH 7.2) containing 1% Tween-20 (PBT 1%; Sigma-Aldrich). PBT containing 5% non-fat dry milk

was used as blocking reagent, and blots were probed with the following antibodies diluted in PBT/1% non-fat milk: alpha 1 spectrin (1:3,000; Abcam, Cambridge, MA), integrin beta 3 (1:1,000; Abcam), myosin smooth muscle heavy chain 1 and 2 (1:10,000; Abcam), and α-actinin (1:3,000; Abcam).

We first planned to use β-actin as a loading control, but the 1-week time points had higher levels of actin in the experimental glaucoma sclera than in the control sclera. We also noted higher actin cytoskeletal signaling in the proteomic data. In contrast, another commonly used control, glyceraldehyde-3-phosphate dehydrogenase (GAPDH), was not altered between the experimental and control tissues in the mean densitometry values; therefore, a mouse monoclonal to rabbit muscle GAPDH was used (1:1,000 dilution, Life Technologies). In the data presented, the ratio of the test molecule to GAPDH on the same membrane is presented.

After overnight probing with primary antibody at 4 °C, membranes were washed in PBT and incubated in the appropriate peroxidase labeled secondary against mouse (KPL, Gaithersburg, MD) or rabbit (KPL), both at 1:10,000 for 1 h at room temperature, and then exposed to enhanced chemiluminescence (ECL) Western Blot Detection Reagent (Amersham/GE HealthCare, Piscattaway, NJ) for 1 min at room temperature. If multiple antibodies were blotted on the same membrane, Restore™ PLUS Western Blot stripping buffer was used (Thermo Scientific) to strip the membranes. Membranes were exposed to Amersham Hyperfilm ECL (Amersham, GE Healthcare Bio-Sciences Pittsburgh, PA), and bands were then quantified using ImageJ software. Background correction was applied to each lane by baseline subtraction, and integral values were selected as measurement parameters. Following normalization to GAPDH, the average values obtained from the normotensive control samples was used to calculate the mean increase in protein expression in the glaucoma scleras, with seven to ten individual scleras per group.

Histological studies:

Whole mounts—Immunohistochemistry studies were performed in all three types of mice, but since the findings did not differ substantially by type of mouse, we present the data for CD1 mice. After IOP elevation, mice were euthanized at 3 days, 1 week, and 6 weeks by exsanguination under general intraperitoneal anesthesia and perfused transcardially with 4% paraformaldehyde in 0.1 M PBS, pH 7.2. The superior pole of each eye was marked for orientation of the specimens, and the eyes were enucleated. Only scleral tissue was harvested. After a series of washes in PBS and PBS containing 0.3% Triton (PBT), the scleras were segmented into quadrants representing superior, nasal, inferior, and temporal positions.

Since the full thickness of an unfixed mouse sclera is less than 50–100 μm and pore size has been shown to allow large molecules to penetrate tissue from both sides, the antibodies penetrated the full thickness of the mouse sclera [24]. For exposure to the primary antibody, the sclera samples were incubated overnight at 4 °C with rabbit anti-Ki67 (Abcam) or mouse α-smooth muscle actin (α-SMA, 1:500; Sigma-Aldrich). The antibodies were diluted in PBT with 10% normal goat serum (NGS). After incubation in the primary antibody solution, the samples were washed in PBT and incubated in appropriate goat anti-rabbit Alexa Fluor 488 secondary for 2 h at room temperature. After final antibody incubation, the nuclei were stained with 4',6-diamidino-2-phenylindole (DAPI; Invitrogen). The scleras were coverslipped with DAKO mounting media (DAKO, Carpenteria, CA).

Tissue sections: Cryosections of optimum cutting temperature (OCT) embedded CD1 tissues were incubated with monoclonal anti-TSP-1 (1:200; Abcam). After overnight incubation in the primary antibody solution and blocking buffer, the samples were exposed to goat anti-mouse Alexa Fluor 568 secondary antibody (1:200; Invitrogen). Finally, the nuclei were counterstained with DAPI (Invitrogen). The samples were coverslipped with DAKO mounting media (DAKO). Scleras and retinas were imaged with a Zeiss LSM 710 Confocal Microscope (Zeiss MicroImaging, Thornwood, NY) at the peripapillary region using a 20X lens. We used two control procedures in the mouse sclera tissue when we used antibodies generated in mice against the molecules studied. First, we blocked immunoglobulin (IgG) labeling with serum, and, second, we treated some control sclera after we omitted the primary antibody as controls. These procedures demonstrated that there was no detectable non-specific labeling. Masked observers graded the amount of Thrombospondin 1 and Hint1 in the scleral sections of the control and glaucomatous tissues. Images were evaluated on a scale of 1–5; 1 was the lowest signal, and 5 was the highest. Individual and average gradings from each observer were statistically analyzed.

DAPI and Ki67 positive quantification: The number of DAPI-labeled nuclei in each scleral whole mount quadrant was quantified using Stereo Investigator software (MicroBrightField, Williston, VT) integrated with an ECLIPSE E600 microscope (Nikon, Japan) with a 3-chip charge-coupled device (CCD) color video camera (HV-C20, Hitachi, Japan) and motorized stage and microcator attachment (Heidenhain EXE 610C, Schaumburg, IL). All DAPI-labeled cells with the

Table 1. First experimental group undergoing proteomic analysis: IOP, axial length, axon loss.

Strain	Time point	Mean difference IOP (mm Hg) ± SD	Axial length increase (mm)±SD (%)	Axial width increase (mm)±SD (%)	Axon count ±SD (%loss)*
CD1	6 weeks	5.7±3.1	2.6±4.3	3.8±5.1	40.0±27.4
	p=	0	0.013	0.001	0.0001
B6	6 weeks	8.0±3.6	8.2±7.5	9.7±7.1	32.3±22.1
	p=	0	0.0001	0	0

elongated shape and ovoid nucleus typical of fibroblasts were counted. Approximately four regions, each 460 µm × 300 µm, were quantified in each quadrant, comprising approximately 4% of the scleral area in a specimen.

Within each designated region, observations were made at three depths through the entire scleral thickness, with each depth comprising a zone approximately 10 µm thick. One depth was near the initial scleral edge, one in the mid-sclera, and one at the opposite scleral edge. Observations made at each of these three depth designations were not significantly different, and therefore, the average is presented. The density of cells per unit area (in DAPI-labeled tissue) and the number and percent labeling positively for Ki67 were analyzed by scleral region (from close to the peripapillary area to the equator), by mouse strain, and by experimental glaucoma compared to control.

Statistical methods: All estimates and p values are from generalized estimating equation (GEE) models, which take into account correlations among repeat measurements by quadrant/region on a single eye. For these models, the outcome variables used were DAPI count, Ki67 count, or the Ki67 count as a percent of the DAPI count. Outcomes were assumed to have a negative binomial distribution. The working correlation matrix for the repeat measurements in four regions in each of four quadrants was assumed to have an exchangeable structure, in which any two repeat measurements have the same correlation.

RESULTS

Proteomic studies: Experimental glaucoma data on IOP, axial length, and RGC axon loss: There were two groups of mice for which proteomic data were obtained. The first group of 18 B6 mice and 19 CD1 mice were studied at 6 weeks after induction of experimental glaucoma. The mean IOP increase (difference between glaucoma and fellow eyes) was significant and did not significantly differ among the mouse strains, B6=8.0±3.6 mmHg; CD1=5.7±3.1 mmHg (p>0.05, *t* test; Table 1; and Appendix 1, Appendix 2). Likewise, the cumulative exposure to elevated IOP over time (positive integral IOP) was not significantly different between strains (p=0.21). At baseline, the CD1 mice had greater axial length than the B6 mice (3.49±0.09 versus 3.30±0.06 mm, p<0.001), as previously reported. In this study, axial length elongation from elevated IOP was significant in both strains and was greater in B6 mice than in CD1 mice (B6: 8.2%, p<0.001 versus CD1: 2.6%, p=0.01; difference between strains, p=0.008). Both strains lost significant numbers of RGC axons at 6 weeks after IOP elevation, 32% and 40%, respectively (both p<0.0001; Table 1; n=18 and 19 scleras in B6 and CD1 mice, respectively). Mean difference IOP was compared to the untreated fellow eye over the time period. The percentage axon loss was the mean compared to pooled controls, and IOP and axial length were compared to the individual fellow control eye; n=5–7 scleras per time point. Data are mean ± standard deviation (SD). The *t* test was used to compare the glaucoma eyes to the control eyes.

The second group of animals studied proteomically included 12 B6 mice (wild-type littermates of Aca23), ten CD1 mice, and 11 Aca23 mice. After experimental IOP increase in one eye, five animals were euthanized from each of the three mouse types at either 1 week or 6 weeks, giving six sets of proteomic data in this group (three strains, two time points each). The second group of mice responded similarly to the first group regarding IOP elevation, axial elongation, and RGC loss, with significantly higher IOP than the control fellow eyes in all three strains by approximately 6–10 mmHg (p<0.01 or less, paired *t* test; Table 2). The baseline axial globe length was shortest in the B6 mice, intermediate in the CD1 mice, and longest in the Aca23 mice, as previously reported [20,21] (p<0.0001, ANOVA). The percent length increase due to experimental glaucoma differed by strain. The Aca23 mice that had longest axial globe at baseline underwent the least elongation (3–4%), while the B6 mice, whose axial globe was shortest at baseline, elongated the most (10% by 6 weeks; Table 2). The RGC loss was lowest in the Aca23 mice (no significant loss) at both time points; however, a smaller number of eyes in each group did not show significant differences among groups.

Table 2. Second experimental group undergoing proteomic analysis: IOP, axial length and axon loss.

Strain	Time	IOP versus control	% axial length Increase	% axon loss
	1 week	6.26 ± 3.0**	6.1±1.7*	13.71±27.7
CD1	6 weeks	5.6 ± 3.3**	9.6±4.0*	−1.5±4.5
	1 week	11.1±7.4**	10.3±0.07**	−5.3±9.9
B6	6 weeks	7.7±3.6**	9.1±7.8**	9.5±15.9
	1 week	5.6±3.7**	3.0 ± 0.03*	−1.5±13.9
Aca23	6 weeks	5.3±4.8**	3.0 ±.04	−10.08±24.0

% axon loss is median compared to pooled controls. IOP is mean difference in IOP compared to untreated fellow eye over the time period. Axial length is compared to individual fellow control eye; n=5 scleras per time point. Data are mean±standard deviation. Minus % axon loss indicates higher number of axons in glaucoma eye than fellow=no damage. *=p<0.05 and **=p<0.01, *t* test comparing glaucoma to fellow eye control.

Proteomic analysis: Canonical pathways changed in experimental glaucoma: Eight proteomic data sets were produced. They were two proteomic data sets at 6 weeks after glaucoma (one from each of two strains) and six data sets, one from each of three strains at two time points, 1 week and 6 weeks. Thus, we had replicate data for 6 weeks after experimental glaucoma induction for the B6 and CD1 mice. A total of 728 molecules increased and 189 decreased among all strains and time points studied, using twofold change as the cutoff (Table 3; and Appendix 3). Bioinformatics analysis of the proteomics data sets with the Ingenuity Pathway Analysis system identified several canonical pathways that were represented more than once (Table 4; Appendix 3). Of the eight sets of data, the pathways most prominently identified as increased in the experimental glaucoma sclera were integrin-linked kinase (ILK) signaling and actin cytoskeleton signaling, both appearing in six of the eight data sets and represented in all three strains of mice and at 1 and 6 weeks (Table 4). Two pathways were found repeatedly changed only in the CD1 mice, at 1 and 6 weeks: protein kinase A and rho family GTPase signaling.

Table 3. Number of sclera proteins exhibiting altered expression in experimental glaucoma.

Strain	Time point	Decreased sclera proteins	Increased sclera proteins	Total
CD1	1 week	125	168	293
	6 weeks	35	275	310
B6	1 week	76	56	132
	6 weeks	31	90	121
Aca23	1 week	8	47	55
	6 weeks	13	92	105

Table 4. Top canonical pathways associated to proteomic data sets.

Pathway	*Frequency	B6	CD1	Aca23	Time Point
Integrin-Linked (ILK) Signaling	6/8 sets	+	+	+	1, 6 weeks
Actin Cytoskeleton Signaling	6/8 sets	+	+	+	1, 6 weeks
Calcium Signaling	3/8 sets	+	-	+	1 week
Cellular Effects of Sildenafil	3/8 sets	+	-	+	1, 6 weeks
Protein Kinase A Signaling	2/8 sets	-	+	-	1,6 weeks
Rho Family GTPase Signaling	2/8 sets	-	+	-	1, 6 weeks

* 8 sets include 1 and 6 weeks for the 3 strains (6 sets) and replicates for B6 and CD1 at 6 weeks (2 sets)

Proteomic analysis: Individual molecules increased in experimental glaucoma sclera: Analysis of molecules that were increased twofold or greater in more than one of the data sets yielded the list shown in Table 5. Several molecules are described below under the general categories of molecules linked by function. A protein that was increased in two of three data sets at 1 week and five of five data sets at 6 weeks after glaucoma was HINT1. Also prominently increased at 1 and 6 weeks in more than one data set was α-actinin 2. Myosin heavy chain 2 was increased in three of three data sets at 1 week, while spectrin α chain was increased in two of two data sets at 1 week. At 6 weeks, parvalbumin α was increased in three of five data sets, while TSP-1 and -4 were increased in two of five data sets at 6 weeks. Venn diagrams are presented in Appendix 4 showing the number of proteins that were increased and decreased in B6 mice, CD1 mice, or both strains, at 1 and 6 weeks. The proteins that were increased in both mouse strains at each time point are listed in Appendix 5.

Actin cytoskeleton and its interaction at the plasma membrane: At 1 week after experimental glaucoma, proteins increased twofold or greater included molecules involved in actin–myosin cytoskeletal mechanisms and their link to membrane components (Appendix 3, group 2 data). Several cytoskeletal-related proteins were increased in two of the three types of mice at 1 week after IOP elevation, including actin-binding LIM protein 1, keratin (cytoskeletal types 1 and 2), kinesin-like protein, plectin, S100A, and vimentin. Others increased in at least one mouse strain were desmin, myosins, nesprin-1, plectin, dynein heavy chain 12, vimentin, α-actinin, myomesin, S100A10, tropomodulin-4, troponin T, tubulin beta, paxillin, kinesin-like protein, plectin, and TRIO (an F-actin-binding protein).

The cytoskeletal proteins increased after 6 weeks of glaucoma in one or more strains included four myosin-related proteins as well as molecules that interact with actin: filamin α and spectrin α2. Also increased were plasminogen (37X higher), echinoderm microtubule-associated protein-like (19X higher), myosin heavy chain 4 (18X), actinin (10xX), cytoskeleton-associated protein 4 (10X), myosin heavy chain 11 (9X), and myosin 1c (4X). The 6-week increase group had examples also elevated at 1 week, such as actin-binding LIM protein, paxillin, kinesin-like protein, plectin, TRIO, and vimentin. Extracellular matrix proteins increased. At 1 week, there was a greater than twofold increase in at least two types of mice for fibrillin 1 and TSP-1 and -4, as well as single strain increases at 1 or 6 weeks in transforming growth factor-beta 1(TGF-β1)-induced transcript 1, plasminogen, TSP-1 precursor, α1 antitrypsin 1, beta-glucuronidase precursor, collagens α1 and 2, lamin-B1, proline synthase, osteoglycin, fibulin-1, perlecan, fibromodulin, and biglycan.

Integrin-linked signaling and cell membrane–associated proteins: At 1 week, the spectrin α chain was elevated in two strains, while individual strains had increased talin 2, β catenin, desmin, and desmoplakin. At 6 weeks, integrins α and β were significantly increased in two mouse strains, along with single strain increases in cadherin-11, clathrin heavy chain 1, desmin, and spectrins α and β, and laminin α2 and β2.

Proteomic analysis: Molecules that significantly decreased: It was substantially less common for proteins to decrease significantly than to increase in all three mice strains. At 1 or 6 weeks, there were lower levels of androgen-binding protein, latent TGF-β-binding protein, plasminogen activator inhibitor 1 RNA-binding protein, β-glucuronidase, clathrin assembly protein, keratocan, S100-A9, tubulin β, and several crystallins. There were also decreases in α galactosidase, caspase 8, fibulin 2, heparin transferase, insulin-like growth factor-binding protein 7, and integrin α and β2 precursor.

Immunoblot data: Immunoblot data were measured for individual scleral specimens with seven to ten eyes each from elevated IOP, fellow control, and naïve bilateral control CD1 animals. The 1-week time period was chosen as having the greater changes in protein expression. Immunoblots were performed with molecules for which there are available and satisfactory antibodies, and which had substantial increases in the proteomic data or were prominent members of the highlighted pathways. For those in which immunoblot confirmation could not be performed, immunofluorescent microscopy of scleral sections was conducted. The immunoblots with myosin smooth muscle heavy chain 1 and 2, sarcomeric α actinin, α1 spectrin, and integrin β3 at 1 week after glaucoma (Figure 1) confirmed the proteomic data for these molecules.

Immunohistochemical labeling: Antibody labeling was performed in scleral whole mounts for α-SMA, vimentin, and actinin and in scleral sections for TSP-1 and HINT1, two proteins that were significantly elevated in the proteomic analysis. We studied four time periods (3 days, 1 week, 3 weeks, and 6 weeks). The 3-day data had the largest differences and are presented here. Labeling for α-SMA at 3 days after IOP elevation was increased in the B6 and CD1 sclera compared to the control eyes in masked evaluation (Figure 2). By 6 weeks after the IOP increase, the masked observer found no consistent differences in α-SMA labeling. Likewise, the masked observer was easily able to detect greater labeling for vimentin and actinin in scleral whole mounts from the 3-day glaucoma eyes than in the control eyes (Figure 2). In the sclera, choroid, and retina cryosections, the labeling for

Table 5. Proteins increased or decreased in 1 or more data sets at 1 or 6 weeks.

Proteins increased	
1 week	**6 weeks**
Up in 3 of 3 data sets	**Up in 5 of 5 data sets**
Myosin heavy chain 2	Histidine triad nucleotide binding protein 1
Up in 2 of 3 data sets	**Up in 3 of 5 data sets**
Acyl-CoA thioesterase 2	Parvalbumin alpha
Alpha-actinin-2	**Up in 2 of 5 data sets**
Centrosomal protein of 170 kDa	Alpha-actinin-2
Fibrillin 1	ATPase, Na^+/K+ transporting, alpha 3 polypeptide
Gamma-crystallin C	Cartilage oligomeric matrix protein
Granulin	Coatomer subunit gamma
Histidine triad nucleotide-binding protein 1	Collagen alpha-3(VI) chain isoform 1 precursor
Maspardin	Cysteine and glycine-rich protein 2
Myosin-1	Fibulin-1 (isoform c)
NADH dehydrogenase [ubiquinone]	Filamin-B
Prostaglandin-H2 D-isomerase	FUS interacting protein 1
Protein Myh15	Granulin
Spectrin alpha chain	Histone H2A
Tripeptidyl-peptidase 1	Histone H4
Vimentin	Integrin beta-3
	Lamin A
	MCG67985
	MCG9909
	Metalloreductase STEAP3
	Myosin-binding protein C
	Paxillin (isoform alpha)
Proteins decreased	
Down in 2 of 3 data sets	**Down in 4 of 5 data sets**
Androgen-binding protein	Androgen-binding protein
Lactotransferrin	**Down in 2 of 5 data sets**
Procollagen-lysine,2-oxoglutarate 5-dioxygenase 1	MCG117626
	Keratin, type II cytoskeletal 1
	Calbindin 2, isoform CRA
	Retinaldehyde binding protein 1

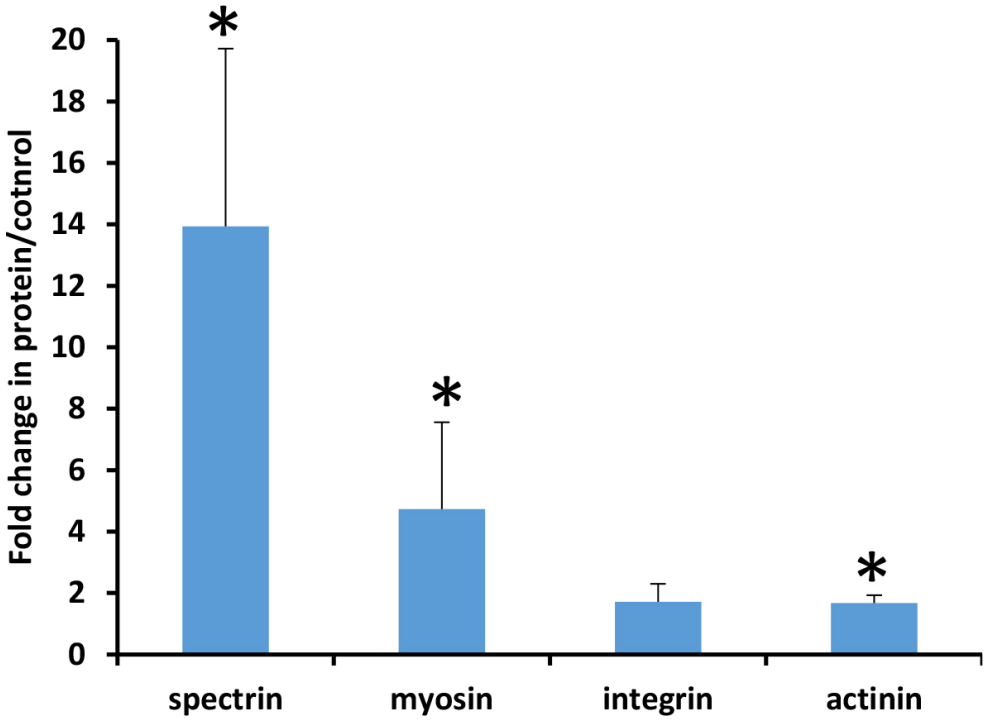

Figure 1. Protein expression changes after 1 week of experimental glaucoma. Immunoblot intensity ratios of experimental glaucoma at 1 week for four selected proteins, with significant elevations in three molecules and all near or greater than twofold increase. Mean ± standard error. Asterisk indicates p value <0.05 for significant increase in glaucoma compared to the control eyes, each referenced to the glyceraldehyde-3-phosphate dehydrogenase (GAPDH) value from the blot; *t* test or Wilcoxon rank-sum test.

TSP-1 was clearly greater in the 3-day glaucoma eyes than in the control eyes, as was the labeling for HINT1 (Figure 3). Interestingly, the TSP-1 labeling was also more prominent in the choroid and retina of 3-day glaucoma eyes than in the control eyes.

TSPs were increased by proteomic analysis, and for this protein, immunolabeling in scleral sections showed a significant increase in masked semiquantitative grading on a 1–5 scale: 3.25±0.25 for the glaucoma eyes and 2.33±0.29 for the control eyes (p=0.002, *t* test; Figure 3). Note that there was a substantial increase in retinal as well as scleral labeling in the glaucoma eyes compared to the healthy eyes. In the HINT1 stained samples, the control sclera averaged a 1.6±0.9 score (1=low, 4=high stain), while the glaucoma sections averaged 3.0±0.6 (statistically significant p≤0.001 (*t* test; Figure 3).

Sclera fibroblast density: We measured cell density (fibroblasts/unit area) in 27 control sclera samples, 13 from CD1 mice and 14 from B6 mice. IOPs were also measured and are shown in Appendix 6. Normal fibroblast mean density, the number of DAPI-labeled nuclei per 0.14 mm^2 field, was 14% greater in the B6 mice than in the CD1 mice (Table 6; multivariable regression). The peripapillary sclera (region R1) had 30% more fibroblasts than the most anterior scleral region (R4), with intermediate density in the two intervening regions (R2 and R3; p=0.001, Table 6, DAPI labeling). The regional mean fibroblast density was lower in the nasal quadrant by 25% compared to the other three quadrants (superior, temporal, and inferior), which did not differ among each other (data not shown). The difference in density between the baseline and 6-week glaucoma scleras was not significant: 548.2±22.1 versus 587.1±23.5 cells/0.14 mm^2 (mean ± standard error; p=0.68, univariate regression, Table 7). In the experimental glaucoma mouse sclera, the fibroblast density was higher in the B6 mice than in the CD1 mice, both at baseline and after glaucoma exposure, but these differences were not significant (n=18 eyes, Table 8). The posterior scleral regions continued to have a significantly higher fibroblast density after experimental glaucoma induction, as they did in controls (Table 8).

Scleral fibroblast proliferation: To evaluate the amount of cell proliferation, we enumerated cells labeled positive for Ki67 per unit area and the percent Ki67 positive among all fibroblasts to take account of differences in fibroblast density across strains or by treatment group. In the control sclera, about 1% of the fibroblasts were Ki67 positive, with no significant differences by mouse strain or scleral region (Table 6). The percent of fibroblasts positive for Ki67 in the experimental glaucoma sclera for all mouse strains increased from 2% in controls to 10% at 1 week and was statistically significantly different from 1 through 6 weeks after induction (Table 7; p=0.0005, univariate regression). Ki67-positive cells were 6 times more common at 1 week and threefold greater at 3 and 6 weeks compared to the control eyes (Table

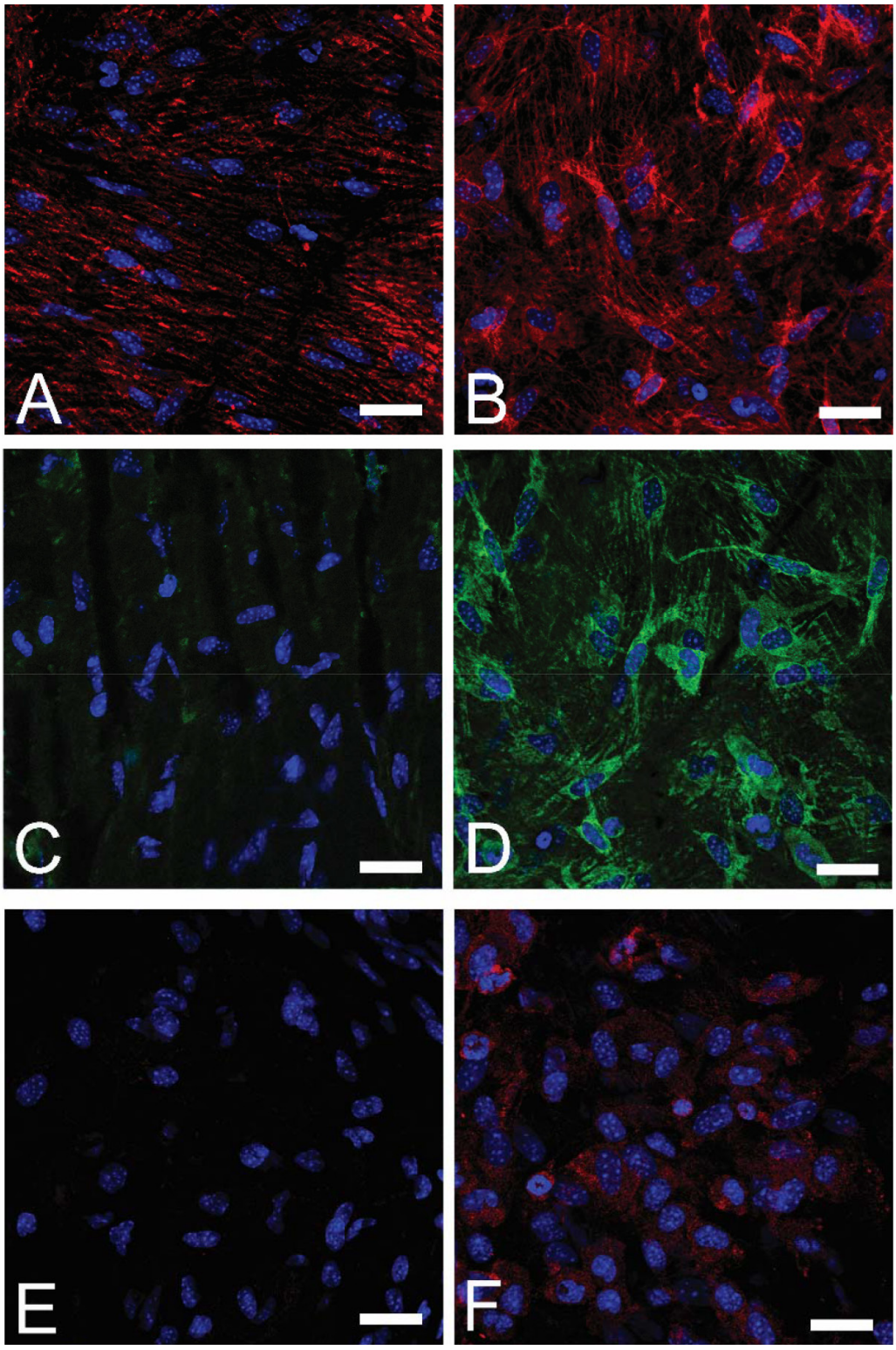

Figure 2. Immunohistochemistry of selected molecules in scleral whole mounts. Immunohistochemistry in whole mounts of sclera for vimentin (red) in (**A**) B6 mouse control and (**B**) 3-day glaucoma sclera cells. **C**, **D**: Control (left) and 3-day glaucoma (right) labeling for α-SMA (B6 mice). **E**, **F**: Control (left) and 3-day glaucoma (right) labeling for cell adhesion molecule, α-actinin (red, CD1 mice). 4',6-diamidino-2-phenylindole (DAPI) nuclear counterstain (blue). Scale bars=20 µm.

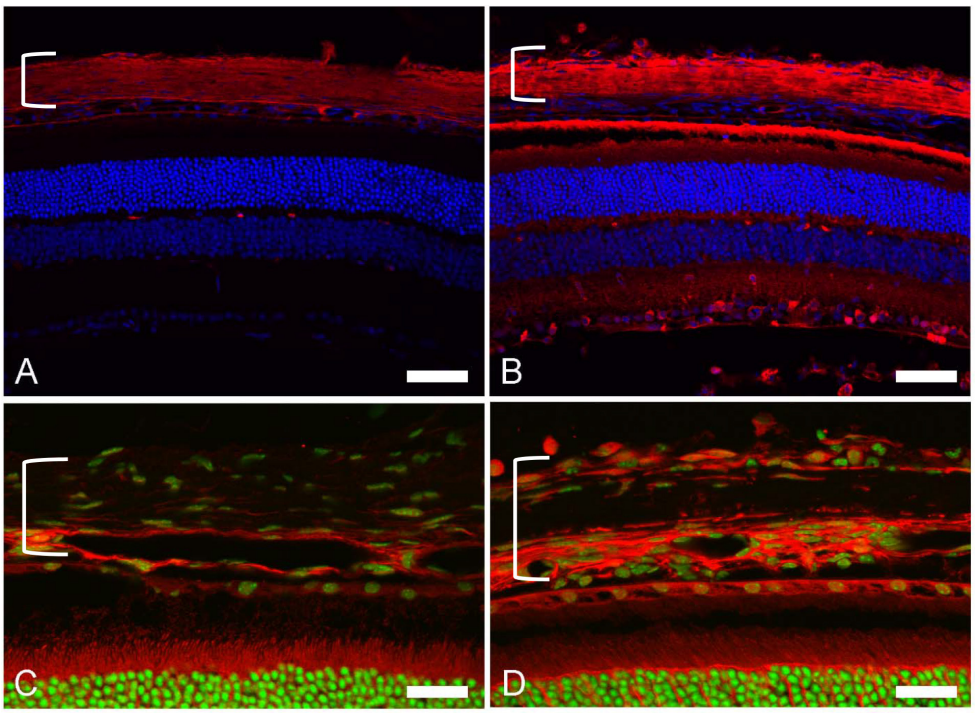

Figure 3. Scleral expression of thrombospondin and HINT1. Immunostaining for thrombospondin-1 (TSP-1; red) counterstained with 4',6-diamidino-2-phenylindole (DAPI; blue) shows labeling comparable to the mean increase in the masked scleral grading (see text). The sclera is marked with a bracket in each panel. **A**: Control. **B**: Increased labeling in the 3-day glaucoma sclera, choroid, and retina (CD1 mice). Scale bar=50 µm. Lower pair shows immunostaining for HINT1 (red), sclera labeling in the (**C**) CD1 control and increased labeling in the glaucoma tissue (**D**). DAPI counterstain (blue in **A**, **B**; green in **C**, **D**). Scale bar=25 µm.

Table 6. Control sclera fibroblast density and proliferation.

Strain	Density				Ki67 positive				% Ki67 positive			
	N	Mean	SE	p	N	Mean	SE	p	N	Mean	SE	p
CD1	92	517.2	(18.6)	0.01	92	4.1	(0.8)	0.48	87	0.9	(0.0)	0,86
B6	96	599.8	(15.7)		96	5.1	(0.6)		94	0.9	(0.1)	
Region	**N**	**Mean**	**SE**	**p**	**N**	**Mean**	**SE**	**p**	**N**	**Mean**	**SE**	**p**
1	47	615.1	(24.6)	0.001	47	5.2	(1.2)	0.96	46	0.9	(0.2)	0.72
2	47	592.4	(21.5)		47	4.7	(0.9)		46	0.8	(0.1)	
3	47	555.7	(20.9)		47	3.9	(0.7)		46	0.7	(0.1)	
4	47	475.0	(27.9)		47	4.6	(1.1)		43	1.2	(0.5)	

*mean=number of cells counted/0.14 mm^2; SE=standard error, n=number of eyes/scleras, C.I.=95% confidence interval

Table 7. Scleral fibroblast proliferation with experimental glaucoma.

Exposure to glaucoma	Density			Ki67 positive			% Ki67 Positive			Ki67 Ratio Glaucoma/Control(C.I.)
	N	Mean	(SE)	N	Mean	(SE)	N	Mean	(SE)	
Control	60	548.2	(22.1)	60	2.0	(0.5)	58	0.3	(0.0)	1
1 Week	40	537.2	(26.0)	40	10.0	(2.2)	39	1.9	(0.4)	6.2 (2.6, 14.7)
3 Weeks	40	586.6	(31.9)	40	6.5	(1.2)	37	1.2	(0.2)	3.5 (1.6, 7.6)
6 Weeks	48	587.1	(23.5)	48	5.6	(1.2)	46	1.0	(0.2)	3.1 (1.1, 8.5)

*mean=number of cells counted/0.14 mm^2; SE=standard error, n=number of eyes/scleras, C.I.=95% confidence interval

Table 8. Fibroblast proliferation by strain and region after experimental glaucoma.

Strain	Density				Ki67 positive				% Ki67 positive			
	N	Mean	SE	p	N	Mean	SE	p	N	Mean	SE	p
CD1	60	549.9	(20.6)	0.6	60	5.7	(0.9)	0.66	58	1.1	(0.1)	0.89
B6	68	588.5	(23.0)		68	8.6	(1.5)		64	1.5	(0.2)	
Region	**N**	**Mean**	**SE**	**p**	**N**	**Mean**	**SE**	**p**	**N**	**Mean**	**SE**	**p**
1	32	582.8	(34.4)	<0.0001	32	5.4	(1.4)	0.37	30	0.9	(0.2)	0.33
2	32	637.8	(22.7)		32	6.5	(1.5)		32	1.2	(0.3)	
3	32	570.4	(21.7)		32	8.6	(2.3)		32	1.5	(0.4)	
4	32	490.6	(38.2)		32	8.4	(1.9)		28	1.7	(0.4)	

*number of cells counted/0.14 mm^2; SE=standard error, n=number of eyes/scleras, C.I.=95% confidence interval

7). Ki67 density and percent Ki67 positive fibroblasts did not differ statistically significantly by strain or by region in the experimental glaucoma eyes overall in a multivariable model (Table 8).

DISCUSSION

The biomechanical stress of experimental glaucoma leads to scleral remodeling through altered fibroblast responses, as judged here by proteomic, immunoblot, and immunohistochemical data. Our proteomic analysis found upregulation in several canonical pathways in experimental glaucoma, particularly for integrin-linked kinase signaling and actin cytoskeleton signaling. This suggests that experimental glaucoma stimulates the activity of the membrane-bound integrins, which link the cytoskeleton to the extracellular matrix. It is likely that extracellular matrix molecules and scleral fibroblasts sense IOP-related stress, at normal and elevated levels of IOP. The observed responses in proteins suggest that cell-mediated and extracellular alterations occur in experimental glaucoma. The cellular component is intimately linked to the extracellular network through a complex of molecules at the cell membrane.

The increases in integrin-linked signal molecules seen here included integrins themselves and paxillin, a signal transduction adaptor related to integrin [36] and TGF-β [37]. Integrins activate the myofibroblast phenotype in corneal fibroblasts [38], and we observed an increase in α-SMA, a feature of myofibroblasts, in the experimental glaucoma sclera. Integrins link scleral fibroblasts to collagen in the scleral matrix [39], mediating IOP-generated stress between the intracellular cytoskeleton and the extracellular matrix. Integrin-linked signaling stimulates TGF-β [40-44], and we found several integrin-related molecules to be increased, including cadherin (a transmembrane protein), clathrin (mediates cell membrane transport), and laminin. A gene array study of scleral fibroblasts in vitro showed increases in cadherin [45] when the cells were stretched. Studies of the optic nerve head in rat glaucoma show increases in gene expression for molecules involved in integrin-linked signaling [46,47].

Molecules related to the actin cytoskeleton and its interaction at the cell membrane were also increased in the experimental glaucoma sclera by proteomic, immunoblot, and histology. Actin-binding LIM protein [48] increased in the proteomic analysis, and α-actinin and spectrin were increased in the proteomic and immunoblot data. The intracellular domain of integrins interacts with actin via actinin [49], a protein in the spectrin superfamily. Spectrin α2 maintains plasma membrane integrity and cytoskeletal structure. Myosins, which interact with actin in cell contraction, were four of the highest elevated molecules according to proteomic analysis, confirmed with immunoblot. This is further evidence that scleral fibroblasts become myofibroblasts. The human sclera is known to have a resident population of myofibroblasts [50], which may increase in response to changes in IOP.

HINT1, the most consistently upregulated protein in our data, has been linked to the pathophysiology of certain psychiatric disorders and exhibits tumor suppressor properties, perhaps related to its effect on intracellular calcium homeostasis [51]. Also known as protein kinase C-interacting protein 1, HINT1 inhibits in fibroblasts the pathway activated by a gene associated with microphthalmia in mice and Waardenburg syndrome in humans, suggesting a role in altering scleral responses [52]. To our knowledge, this pathway had not been previously studied or identified as important in glaucoma, but clearly deserves investigation.

Fibroblasts occupy 25% of the scleral thickness in fixed mouse sclera [23], normally residing within their own layers, which alternate with cell-free, collagenous lamellae. Fibroblast density in scleral whole mounts was about 4,000 cells per mm^3, leading to an estimated 75,000 fibroblasts overall in the mouse sclera. Thus, it is not surprising that these cells play an important role in the ocular response to experimental glaucoma and other processes that affect the sclera. Scleral fibroblasts have the elongated shape and positive labeling for vimentin characteristic of mesenchymally-derived fibroblasts. In the control sclera, <1% of fibroblasts prepared for cell division (Ki67 positive). The rate of division increased with experimentally elevated IOP, continuing at a higher than usual rate for weeks. In a companion report, we found that the volume of cellular scleral lamellae increased as a proportion of scleral thickness after experimental glaucoma [23]. We did not detect a statistically significant increase in the density of fibroblasts in experimental glaucoma eyes. Possibly, the increase due to cell division is insufficient to produce an overall increase in density, or the increased cell number by division is balanced by cell death. Alternatively, changes in non-cellular scleral components may alter the overall tissue volume to mask an increase in cell number. We found that the non-fibrillar components of sclera decrease in fresh tissue thickness measured in experimental mouse glaucoma [23]; thus, there are substantial changes in major scleral elements.

In models of experimental myopia, the axial length of the sclera increases in response to form deprivation or image blur. Likewise, in experimental glaucoma, the sclera elongates rapidly after increases in IOP. Superficially, it might be expected that scleral elongation in the two conditions would result from similar biochemical and cellular changes. However, our data show, for the first time, that alterations of the sclera are in opposing directions in myopia and glaucoma despite both leading to enlargement of the sclera. For example, developing myopia is associated with increased elasticity and increased creep rate [53], while experimental and human glaucoma eyes demonstrate decreases in mechanical compliance [54]. Although the sclera thins in myopia, due to decreased production and degradation of collagen and proteoglycans [55], human glaucoma eyes with RGC damage have thicker sclera [18] (in fixed tissue sections) than age-matched controls. Proteomic changes in the ocular expansion phase of experimental tree shrew myopia show decreases in TSP-1 [56], compared to increases in experimental glaucoma. Integrins decrease in the induced myopia elongation phase in the tree shrew [33], while integrin-related signaling increases in experimental glaucoma. In experimental myopia in the guinea pig [57], there was a decrease in fibroblasts in the posterior sclera, while we found increased cell division and a non-significant increase in cell density. Thus, myopic scleral elongation exhibits distinctly different features from that observed with elevated IOP, both achieving axial elongation, but by different mechanisms.

An important central molecule implicated in our data is TGF-β. Increased extracellular proteins related to TGF-β or its effects included TSP, plasminogen, fibromodulin, fibulin-1, perlecan, and heparin sulfate proteoglycan. TSPs were increased in experimental glaucoma sclera according to proteomic and immunoblot analysis. These large trimeric extracellular glycoproteins participate in wound healing, angiogenesis, and cell adhesion [58,59] and are involved in transforming corneal keratocytes into myofibroblasts after wounding [60]. TSP is a potent activator of TGF-β1 [61,62] which is known to stimulate fibroblast proliferation in the cornea, induce the transition to myofibroblasts, and alter extracellular matrix production [63]. Proteomic data indicated a prolonged elevation of plasminogen, an activator of collagenase that interacts with TSP and fibronectin. Fibromodulin, a small interstitial proteoglycan, participates in the assembly of the extracellular matrix and regulates TGF-β activity [64]. Fibulin-1 is a secreted glycoprotein that is found in association with extracellular matrix structures and binds to extracellular matrix constituents, including fibronectin and versican. Perlecan is a potent inhibitor of smooth muscle cell proliferation and promotes fibroblast growth factor 2 activity. Biglycan is a small leucine-rich repeat proteoglycan (SLRP) that interacts with collagen. Stretching of lamina cribrosa cells in vitro produces similar increases in TSP-1, perlecan, lysyl oxidase, TGF-β2, biglycan, and versican [65]. We have recently shown that inhibition of TGF-β signaling by inhibition of angiotensin 2 type 1 receptors with losartan is neuroprotective in experimental glaucoma [25]. Further study of this area could be therapeutically useful.

We studied three mice strains in the present report, since our cited work has suggested differential susceptibility to experimental glaucoma damage among mouse strains. The initial analysis did not provide strain-specific findings in the response of scleral fibroblasts or proteomic results. This could mean that each strain responds similarly or that the methods used were too general to identify more detailed differences. Now that we have been made aware through the proteomic findings of specific pathways of interest, we plan further work to study differences by strain in important molecular changes in the sclera.

There are inherent limitations in proteomic analysis that should be taken into account. Measurement of the amounts of a protein depends on the identification of some portion of the molecule and often in tiny amounts. Even with three identifiers for each protein and overall replicates, as we performed here, conservative conclusions are merited except large changes or alterations in biochemical pathways in which several associated proteins are identified. Simply because a protein is increased or decreased in amount does not signify a change in the effect of the protein in tissues, since many molecules must be in an active form to be effective. For many molecules, multiple isoforms or assemblies have related and differing properties.

In these data, we compared eyes with induced higher IOP to their fellow eyes in the proteomic analysis. In some research, interventions on one eye affected the untreated fellow eye. In the immunoblot confirmations in this report, we used bilaterally naïve eyes as controls to confirm that the proteomic findings in important molecules were unaffected by contralateral effects. In past research with rodent glaucoma models, we have seen such effects in untreated fellow eyes, though these effects were more prominent in retinal gene array data after optic nerve transection than after experimental glaucoma [66]. We are unaware of data suggesting that the fellow eye sclera would be affected by experimental glaucoma in the other eye. If there were such contralateral effects, then differences between the eyes would be decreased, assuming that the effects were in the same direction in fellow eyes as in treated eyes. Thus, it would make it less likely that we would find significant differences as were seen here.

In summary, experimental glaucoma induces alterations in the mouse sclera that include increased fibroblast division, transition to features of a myofibroblast phenotype, and activation of proteins involved in integrin-linked signaling and actin cytoskeletal pathways. The direction of change in many features of sclera in experimental glaucoma was opposite from that seen in experimental myopia. TGF-β signaling was identified in our data to be associated with experimental glaucoma. This pathway has previously been involved in trabecular meshwork [67] and optic nerve head responses in glaucoma [68,69]. It is likely that more detailed studies of this area will yield important insights into glaucoma effects, as well as potential therapeutic approaches to minimize RGC death.

APPENDIX 1. IOPS OF ‘GROUP 1’

Legend: Mean IOP of proteomics ‘Group 1’ of CD1 and B6 both strains combined. Dotted line represents glaucoma eyes, solid line represents fellow control eyes. Asterisks=significant difference by *t* tests. To access these data, click or select the words "Appendix 1".

APPENDIX 2. IOPS OF ‘GROUP 2’

Legend: Mean IOP of proteomics ‘Group 2’, Aca23, B6, CD1, for all strains combined. Dotted line represents glaucoma eyes, solid line represents fellow control eyes. To access these data, click or select the words "Appendix 2".

APPENDIX 3. PROTEINS INCREASED IN GLAUCOMA

To access these data, click or select the words "Appendix 3".

APPENDIX 4. VENN DIAGRAMS OF NUMBER OF PROTEINS DECREASED (RED) AND INCREASED (GREEN) AFTER 1 WEEK AND 6 WEEKS EXPOSURE TO GLAUCOMA IN B6 AND CD1 MICE.

To access these data, click or select the words "Appendix 4".

APPENDIX 5. PROTEINS INCREASED IN MULTIPLE MOUSE STRAINS

To access these data, click or select the words "Appendix 5".

APPENDIX 6. IOPS OF FIBROBLAST COUNTED SCLERAS

Legend: Mean IOP of fibroblast counted eyes of Aca23 KO, B6, CD1 strains combined. Dotted line represents glaucoma eyes, solid line represents fellow control eyes. To access these data, click or select the words "Appendix 6".

ACKNOWLEDGMENTS

This work was supported in part by Public Health Service Research Grants (PHS), EY02120 and P30EY01765 (Dr Quigley, and Wilmer Institute Core grant) and by unrestricted support from Saranne and Livingston Kosberg and from William T. Forrester. The funders had no role in study design, data collection and analysis, decision to publish, or preparation of the manuscript.

REFERENCES

1. Burgoyne CF, Downs JC, Bellezza AJ, Suh JK, Hart RT. The optic nerve head as a biomechanical structure: a new paradigm for understanding the role of IOP-related stress and strain in the pathophysiology of glaucomatous optic nerve head damage. Prog Retin Eye Res 2005; 24:39-73. [PMID: 15555526].
2. Sigal IA, Yang H, Roberts MD, Burgoyne CF, Downs JC. IOP-induced lamina cribrosa displacement and scleral canal expansion: an analysis of factor interactions using parameterized eye-specific models. Invest Ophthalmol Vis Sci 2011; 52:1896-907. [PMID: 20881292].
3. Sigal IA, Flanagan JG, Ethier CR. Factors influencing optic nerve head biomechanics. Invest Ophthalmol Vis Sci 2005; 46:4189-99. [PMID: 16249498].
4. Quigley HA, Addicks EM, Green WR, Maumenee AE. Optic nerve damage in human glaucoma. II. The site of injury and susceptibility to damage. Arch Ophthalmol 1981; 99:635-49. [PMID: 6164357].
5. Silver DM, Geyer O. Pressure-volume relation for the living human eye. Curr Eye Res 2000; 20:115-20. [PMID: 10617912].
6. Girard MJA, Suh JK, Bottlang M, Burgoyne C, Downs JC. Scleral biomechanics in the aging monkey eye. Invest Ophthalmol Vis Sci 2009; 50:5226-37. [PMID: 19494203].
7. Young RD. The ultrastructural organization of proteoglycans and collagen in human and rabbit sclera matrix. J Cell Sci 1985; 74:94-104. .
8. Watson PG, Young RD. Scleral structure, organization and disease. A review. Exp Eye Res 2004; 78:609-23. [PMID: 15106941].
9. Komai Y, Ushiki T. The three dimensional organization of collagen fibrils in the human cornea and sclera. Invest Ophthalmol Vis Sci 1991; 32:2244-58. [PMID: 2071337].
10. Myers KM, Cone FE, Quigley HA, Gelman SE, Pease ME, Nguyen TD. The in vitro inflation response of mouse sclera. Exp Eye Res 2010; 91:866-75. [PMID: 20868685].
11. Downs JC, Yang H, Girkin C, Sakata L, Bellezza A, Thompson H, Burgoyne CF. Three-dimensional histomorphometry of the normal and early glaucomatous monkey optic nerve head: Neural canal and subarachnoid space architecture. Invest Ophthalmol Vis Sci 2007; 48:3195-208. [PMID: 17591889].
12. Girard MJ, Suh JK, Bottlang M, Burgoyne CF, Downs JC. Biomechanical changes in the sclera of monkey eyes exposed to chronic IOP elevations. Invest Ophthalmol Vis Sci 2011; 52:5656-69. [PMID: 21519033].
13. Girard MJ, Suh JK, Bottlang M, Burgoyne CF, Downs JC. Scleral biomechanics in the aging monkey eye. Invest Ophthalmol Vis Sci 2009; 50:5226-37. [PMID: 19494203].
14. Coudrillier B, Tian J, Alexander S, Myers KM, Quigley HA, Nguyen TD. Biomechanics of the human posterior sclera: age- and glaucoma-related changes measured using inflation testing. Invest Ophthalmol Vis Sci 2012; 53:1714-28. [PMID: 22395883].
15. Urban Z, Agapova O, Hucthagowder V, Yang P, Starcher BC, Hernandez MR. Population differences in elastin matauration in optic nerve head tissue and astrocytes. Invest Ophthalmol Vis Sci 2007; 48:3209-15. [PMID: 17591890].
16. Olsen TW, Edelhauser HF, Lim JI, Geroski DH. Human scleral permeability. Effects of age, cryotherapy, transscleral diode laser, and surgical thinning. Invest Ophthalmol Vis Sci 1995; 36:1893-903. [PMID: 7543465].
17. Thorleifsson G, Magnusson KP, Sulem P. Walters Gb, Gudbjartsson DF, Stefansson H, Jonsson T, Jonasdottir A, Jonasdottir A, Stefansdottir G, Masson G, Gudmundur HA, Petursson H, Arnarsson A, Motallebipour M, Wallerman O, Wadelius C, Gulcher JR, Thorsteinsdottir U, Kong A, Jonasson F, Stefansson K. Common sequence variants in the LOXL1 gene confer susceptibility to exfoliation glaucoma. Science 2007; 317:1397-400. [PMID: 17690259].
18. Gottanka J, Flugel-Koch C, Martus P, Johnson DH, Lütjen-Drecoll E. Correlation of psydoexfoliative material and optic nerve damage in pseudoexfoliation syndrome. Invest Ophthalmol Vis Sci 1997; 38:2435-46. [PMID: 9375560].
19. Cone FE, Steinhart MR, Oglesby EN, Kalesnykas G, Pease ME, Quigley HA. The effects of anesthesia, mouse strain and age on intraocular pressure and an improved murine model of experimental glaucoma. Exp Eye Res 2012; 99:27-35. [PMID: 22554836].
20. Cone FE, Gelman SE, Son JL, Pease ME, Quigley HA. Differential susceptibility to experimental glaucoma among 3 mouse strains using bead and viscoelastic injection. Exp Eye Res 2010; 91:415-24. [PMID: 20599961].
21. Steinhart MR, Cone FE, Nguyen C, Nguyen TD, Pease ME, Puk O, Graw J, Oglesby E, Quigley HA. Mice with an induced mutation in Collagen 8A2 develop larger eyes and are resistant to retinal ganglion cell damage in an experimental glaucoma model. Mol Vis 2012; 18:1093-106. [PMID: 22701298].
22. Steinhart MR, Cone-Kimball E, Nguyen C, Nguyen TD, Pease ME, Chakravarti S, Oglesby EN, Quigley HA. Susceptibility to glaucoma damage related to age and connective tissue mutations in mice. Exp Eye Res 2014; 119:54-60. [PMID: 24368172].
23. Cone-Kimball E, Nguyen C, Oglesby EN, Pease ME, Steinhart MR, Quigley HA. Scleral structural alterations associated with chronic experimental IOP elevation in mice. Mol Vis 2013; 19:2023-39. [PMID: 24146537].
24. Pease ME, Oglesby EN, Cone-Kimball E, Steinhart MR, Hanes J, Kim A, Quigley HA. Scleral diffusivity varies by mouse strain and is decreased by chronic experimental glaucoma. Invest Ophthalmol Vis Sci 2014; 55:2564-73. [PMID: 24557355].
25. Quigley HA, Pitha IF, Welsbie DS, Nguyen C, Steinhart MR, Nguyen TD, Pease ME, Oglesby EN, Berlincke CA, Mitchell KL, Kim J, Jefferys JJ, Kimball EC. Losartan treatment protects retinal ganglion cells and alters scleral remodeling in experimental glaucoma. PLoS One 2015; 10:10-e0141137[PMID: 26505191].

26. Levkovitch-Verbin H, Quigley HA, Martin KR, Valenta D, Baumrind LA, Pease ME. Translimbal laser photocoagulation to the trabecular meshwork as model of glaucoma in rats. Invest Ophthalmol Vis Sci 2002; 43:402-10. [PMID: 11818384].

27. Tezel G, Yang X, Luo C, Cai J, Kain AD, Powell DW, Kuehn MH, Pierce WM. Hemoglobin expression and regulation in glaucoma: insights into retinal ganglion cell oxygenation. Invest Ophthalmol Vis Sci 2010; 51:907-19. [PMID: 19741249].

28. Yang X, Luo C, Cai J, Powell DW, Yu D, Kuehn MH, Tezel G. Neurodegenerative and inflammatory pathway components linked to TNF-alpha/TNFR1 signaling in the glaucomatous human retina. Invest Ophthalmol Vis Sci 2011; 52:8442-54. [PMID: 21917936].

29. Tezel G, Yang X, Luo C, Cai J, Powell DW. An astrocyte-specific proteomic approach to inflammatory responses in experimental rat glaucoma. Invest Ophthalmol Vis Sci 2012; 53:4220-33. [PMID: 22570341].

30. Yao X, Freas A, Ramirez J, Demirev PA, Fenselau C. Proteolytic 18O labeling for comparative proteomics: model studies with two serotypes of adenovirus. Anal Chem 2001; 73:2836-42. [PMID: 11467524].

31. Heller M, Mattou H, Menzel C, Yao X. Trypsin catalyzed 16O-to-18O exchange for comparative proteomics: tandem mass spectrometry comparison using MALDI-TOF, ESI-QTOF, and ESI-ion trap mass spectrometers. J Am Soc Mass Spectrom 2003; 14:704-18. [PMID: 12837592].

32. Miyagi M, Rao KC. Proteolytic 18O-labeling strategies for quantitative proteomics. Mass Spectrom Rev 2007; 26:121-36. [PMID: 17086517].

33. Yang X, Hondur G, Li M, Cai J, Klein JB, Kuehn MH, Tezel G. Proteomics analysis of molecular risk factors in the ocular hypertensive human retina. Invest Ophthalmol Vis Sci 2015; 56:5816-30. [PMID: 26348630].

34. Mann M, Kelleher NL. Precision proteomics: the case for high resolution and high mass accuracy. Proc Natl Acad Sci USA 2008; 105:18132-8. [PMID: 18818311].

35. Tezel G. A proteomics view of the molecular mechanisms and biomarkers of glaucomatous neurodegeneration. Prog Retin Eye Res 2013; 35:18-43. [PMID: 23396249].

36. Turner CE. Paxillin. Int J Biochem Cell Biol 1998; 30:955-9. [PMID: 9785458].

37. Meyer-ter-Vehn T, Han H, Grehn F, Schlunck G. Extracellular matrix elasticity modulates TGF-β–induced p38 activation and myofibroblast transdifferentiation in human tenon fibroblasts. Invest Ophthalmol Vis Sci 2011; 52:9149-55. [PMID: 22058331].

38. Jester JV, Huang J, Fisher S, Spiekerman J, Chang JH, Wright WE, Shay JW. Myofibroblast differentiation of normal human keratocytes and hTERT, extended-life human corneal fibroblasts. Invest Ophthalmol Vis Sci 2003; 44:1850-8. [PMID: 12714615].

39. Shelton L, Summers Rada JA. Inhibition of human scleral fibroblast cell attachment to collagen type I by TGFBIp. Invest Ophthalmol Vis Sci 2009; 50:3542-52. [PMID: 19387070].

40. Nakerakanti SS, Bujor AM, Trojanowska M. CCN2 is required for the TGF-β induced activation of Smad1-Erk1/2 signaling network. PLoS One 2011; 6:e21911-[PMID: 21760921].

41. Scaffidi AK, Petrovic N, Moodley YP, Fogel-Petrovic M, Kroeger KM, Seeber RM, Eidne KA, Thompson PJ, Knight DA. Alpha(v)beta(3) integrin interacts with the transforming growth factor beta (TGFbeta) type II receptor to potentiate the proliferative effects of TGFbeta1 in living human lung fibroblasts. J Biol Chem 2004; 279:37726-33. [PMID: 15187087].

42. Hu S, Cui D, Yang X, Hu J, Wan W, Zeng J. The crucial role of collagen-binding integrins in maintaining the mechanical properties of human scleral fibroblasts-seeded collagen matrix. Mol Vis 2011; 17:1334-42. [PMID: 21647271].

43. Jester JV, Huang J, Fisher S, Spiekerman J, Chang JH, Wright WE, Shay JW. Myofibroblast differentiation of normal human keratocytes and hTERT, extended-life human corneal fibroblasts. Invest Ophthalmol Vis Sci 2003; 44:1850-8. [PMID: 12714615].

44. McBrien NA, Metlapally R, Jobling AI, Gentle A. Expression of collagen-binding integrin receptors in the mammalian sclera and their regulation during the development of myopia. Invest Ophthalmol Vis Sci 2006; 47:4674-82. [PMID: 17065473].

45. Cui W, Bryant MR, Sweet PM, McDonnell PJ. Changes in gene expression in response to mechanical strain in human scleral fibroblasts. Exp Eye Res 2004; 78:275-84. [PMID: 14729359].

46. Morrison JC. Integrins in the optic nerve head: potential roles in glaucomatous optic neuropathy (an American Ophthalmological Society thesis). *Trans Am Ophthalmol Soc.* 2006;104:453–477.

47. Johnson EC, Jia L, Cepurna WO, Doser TA, Morrison JC. Global changes in optic nerve head gene expression after exposure to elevated intraocular pressure in a rat glaucoma model. Invest Ophthalmol Vis Sci 2007; 48:3161-77. [PMID: 17591886].

48. Olson EN, Nordheim A. Linking actin dynamics and gene transcription to drive cellular motile functions. Nat Rev Mol Cell Biol 2010; 11:353-65. [PMID: 20414257].

49. McBrien NA, Gentle A. Role of the sclera in the development and pathological complications of myopia. Prog Retin Eye Res 2003; 22:307-38. [PMID: 12852489].

50. Poukens V, Glasgow BJ, Demer JL. Nonvascular contractile cells in sclera and choroid of humans and monkeys. Invest Ophthalmol Vis Sci 1998; 39:1765-74. [PMID: 9727398].

51. Linde CI, Feng B, Wang JB, Golovina VA. Histidine triad nucleotide-binding protein 1 (HINT1) regulates Ca(2+) signaling in mouse fibroblasts and neuronal cells via

store-operated Ca(2+) entry pathway. Am J Physiol Cell Physiol 2013; 304:C1098-104. [PMID: 23576580].

52. Razin E, Zhang ZC, Nechushtan H, Frenkel S, Lee YN, Arudchandran R, Rivera J. Suppression of microphthalmia transcriptional activity by its association with protein kinase C-interacting protein 1 in mast cells. J Biol Chem 1999; 274:34272-6. [PMID: 10567402].

53. McBrien NA, Jobling AI, Gentle A. Biomechanics of the sclera in myopia: Extracellular and cellular factors. Optom Vis Sci 2009; 86:E23-30. [PMID: 19104466].

54. Nguyen C, Cone FE, Nguyen TD, Coudrillier B, Pease ME, Steinhart MR, Oglesby EN, Jefferys JL, Quigley HA. Studies of scleral biomechanical behavior related to susceptibility for retinal ganglion cell loss in experimental glaucoma. Invest Ophthalmol Vis Sci 2013; 54:1767-80. [PMID: 23404116].

55. Norton TT, Rada JA. Reduced extracellular matrix in mammalian sclera with induced myopia. Vision Res 1995; 35:1271-81. [PMID: 7610587].

56. Gao H, Frost MR, Siegwart JT, Norton TT. Patterns of mRNA and protein expression during minus-lens compensation and recovery in tree shrew sclera. Mol Vis 2011; 17:903-19. [PMID: 21541268].

57. Backhouse S, Phillips JR. Effect of induced myopia on scleral myofibroblasts and in vivo ocular biomechanical compliance in the guinea pig. Invest Ophthalmol Vis Sci 2010; 51:6162-71. [PMID: 20592231].

58. Bornstein P. Thrombospondins as matricellular modulators of cell function. J Clin Invest 2001; 107:929-34. [PMID: 11306593].

59. Lawler J. The functions of thrombospondin-1 and-2. Curr Opin Cell Biol 2000; 12:634-40. [PMID: 10978901].

60. Matsuba M, Hutcheon AE, Zieske JD. Localization of thrombospondin-1 and myofibroblasts during corneal wound repair. Exp Eye Res 2011; 93:534-40. [PMID: 21749870].

61. Young GD, Murphy-Ullrich JE. Molecular interactions that confer latency to transforming growth factor-beta. J Biol Chem 2004; 279:38032-9. [PMID: 15208302].

62. Bornstein P. Thrombospondins function as regulators of angiogenesis. J Cell Commun Signal 2009; 3:189-200. [PMID: 19798599].

63. Jester JV, Petroll WM, Cavanagh HD. Corneal stromal wound healing in refractive surgery: the role of myofibroblasts. Prog Retin Eye Res 1999; 18:311-56. [PMID: 10192516].

64. Chakravarti S, Paul J, Roberts L, Chervoneva I, Oldberg A, Birk DE. Ocular and scleral alterations in gene-targeted lumican-fibromodulin double-null mice. Invest Ophthalmol Vis Sci 2003; 44:2422-32. [PMID: 12766039].

65. Kirwan RP, Fenerty CH, Crean J, Wordinger RJ, Clark AF, O'Brien CJ. Influence of cyclical mechanical strain on extracellular matrix gene expression in human lamina cribrosa cells in vitro. Mol Vis 2005; 11:798-810. [PMID: 16205625].

66. Yang Z, Quigley HA, Pease ME, Yang Y, Qian J, Valenta D, Zack DJ. Changes in gene expression in experimental glaucoma and optic nerve transection: The equilibrium between protective and detrimental mechanisms. Invest Ophthalmol Vis Sci 2007; 48:5539-48. [PMID: 18055803].

67. Prendes MA, Harris A, Wirostko BM, Gerber AL, Siesky B. The role of transforming growth factor β in glaucoma and the therapeutic implications. Br J Ophthalmol 2013; 97:680-6. [PMID: 23322881].

68. Lukas TJ, Miao H, Chen L, Riordan SM, Li W, Crabb AM, Wise A, Du P, Lin SM, Hernandez MR. Susceptibility to glaucoma: differential comparison of the astrocyte transcriptome from glaucomatous African American and Caucasian American donors. Genome Biol 2008; 9:R111-[PMID: 18613964].

69. Fuchshofer R, Tamm ER. The role of TGF-β in the pathogenesis of primary open-angle glaucoma. Cell Tissue Res 2012; 347:279-90. [PMID: 22101332].

Articles are provided courtesy of Emory University and the Zhongshan Ophthalmic Center, Sun Yat-sen University, P.R. China. The print version of this article was created on 29 January 2016. This reflects all typographical corrections and errata to the article through that date. Details of any changes may be found in the online version of the article.